Journal of Applied Fluid Mechanics, Vol. 18, No. 2, pp. 304-316, 2025.
Available online at www.jafmonline.net, ISSN 1735-3572, EISSN 1735-3645.
https://doi.org/10.47176/jafm.18.2.2889

CFD Analysis of Straightener Designs on Overall Performance of the Axial Flow Blood Pump

P. K. Shukla[1†], R. Mishra[2] and R. P. Tewari[1]

[1] *Department of Applied Mechanics, Motilal Nehru National Institute of Technology Allahabad, Prayagraj-211004, India*
[2] *School of Computing and Engineering, University of Huddersfield, Huddersfield, U.K.*

†*Corresponding Author Email: pravin.2015ram07@mnnit.ac.in*

ABSTRACT

Ventricular assist devices (VADs) have emerged as an effective clinical tool for offering crucial aid to patients suffering with heart failure. To achieve optimal performance that matches a healthy ventricle, precise design and a thorough understanding of hydraulic and clinical factors are crucial. This research paper presents a comprehensive analysis using computational fluid dynamics (CFD) software ANSYS Fluent at different range of rotational speed and flow rate to examine the performance of an axial blood pump with three different straightener designs: conical, cylindrical, and paraboloid. The primary objective is to assess the impact of these straightener designs on the overall performance of the axial blood pump. Initially, the base axial pump employed conical straightener designs, which were subsequently modified to paraboloid and cylindrical shapes to evaluate their performance. Consistently, the results demonstrated that the paraboloid design outperformed the other designs. Specifically, the axial blood pump equipped with a paraboloid straightener exhibited an increased pressure head and lower intensity of turbulent kinetic energy compared to the other two designs. Additionally, the wall shear stress in the impeller region was lower in the paraboloid design. By employing CFD tool, this study provides valuable insights into the performance of different straightener designs for axial blood pumps. The findings highlight the superiority of the paraboloid design in terms of pressure head and wall shear stress reduction. These results contribute to enhancing the effectiveness and efficiency of left ventricular assist devices (LVADs), ultimately benefiting patients with heart failure.

Article History

Received June 7, 2024
Revised September 10, 2024
Accepted September 15, 2024
Available online December 4, 2024

Keywords:

VADs
CVDs
Heart failure
Wall shear stress
Hemodynamic complications

1. INTRODUCTION

Cardiovascular diseases (CVDs) contribute significantly to global mortality rates (Valledor et al., 2024). The limited availability of heart donors for transplantation has led to an increased demand for alternative treatment options (Jou et al., 2024). VADs have emerged as successful tools in providing life-saving assistance to patients with severe heart failure (Tu et al., 2024). VADs, essentially mechanical pumps, can be categorized into two main types: pulsatile or continuous. Pulsatile VADs aim to replicate the natural rhythm of the heart. However, due to their bulky size and numerous moving components, they are typically employed for short-term support (Wu et al., 2020). On the other hand, continuous-flow VADs, characterized by their smaller size and fewer moving parts, are suitable for long-term support. They also exhibit less hemodynamic complexity compared to pulsatile VADs (Noly et al., 2020).

The components of an LVAD such as straighter, impeller and diffuser play a pivotal role in generating adequate blood flow to support the failing heart (Mani et al., 2021). The numerous research articles have primarily concentrated on the impeller and diffuser of LVADs to enhance their overall performance (Untaroiu et al., 2005; Qi et al., 2012; Peng et al., 2014; Kannojiya et al., 2019). Existing research on blood pumps has utilized various straightener designs, as documented in several studies (Su et al., 2012; Kannojiya et al., 2019; Yang et al., 2022; Xiang et al., 2023). These studies have primarily focused on enhancing clinical and hydraulic performance aspects, concentrating on boundary conditions or other components such as impellers and diffusers. However, the impact of different straightener geometries remains largely unexplored. Therefore, the straightener component of LVADs is equally vital and cannot be overlooked.

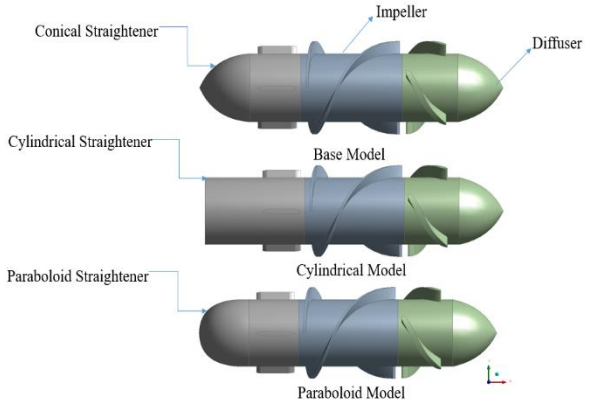

(a) Blood pump design with different straighteners

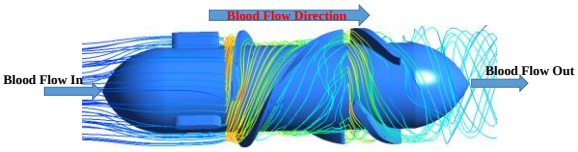

(b) Blood flow dynamics in the pump

Fig. 1 Blood pump with components and flow dynamics

Straighteners play a crucial role in minimizing flow disruptions and ensuring a smooth and consistent flow pattern through the pump. The design of straighteners significantly impacts the pump's overall performance and its capacity to deliver effective mechanical circulatory support.

In recent years, CFD simulations have become invaluable tools for analyzing and optimizing the performance of axial blood pumps. These simulations provide a detailed understanding of fluid flow patterns, pressure distributions, and shear stresses within the pump, enabling researchers to assess the effectiveness of different design configurations (Shukla et al., 2023).

This research article focuses on conducting a comprehensive analysis of axial flow VAD using CFD tool to investigate the impact of different straightener designs on the overall performance of this axial blood pump. The study involves comparing three straightener designs: conical, paraboloid, and cylindrical. The conical design serves as the baseline, while the paraboloid and cylindrical designs are modifications made for comprehensive performance evaluation. This research enhances understanding of straightener design's impact on axial blood pump performance, aiding in the development of more efficient VADs for improved patient outcomes in heart failure.

2. MATERIALS AND METHODS

CFD tools provide detailed insights into fluid dynamics characteristics within blood pumps, aiding in design optimization and performance enhancement (Cheng et al., 2021; Yang et al., 2022; Shukla et al., 2023). ANSYS Fluent software has been used for precise simulation of blood pumps for hydraulic and clinical performance evaluation.

2.1 Blood Pump Geometry and Operation

The geometry of the axial blood pump, specifically VADs, considered in this study was designed using SolidWorks software. Figure 1, illustrates the schematic diagram of the axial blood pump base model, along with two modified models where the straightener was altered to cylindrical and paraboloid shapes. The base design of the present model draws inspiration from the work of Su et al. (2012), with certain unavailable features assumed based on engineering judgment and relevant literature. The pump's base model is designed to meet necessary physiological requirements, such as a 100 mmHg pressure head and a 5 L/min flow rate (Bounouib et al., 2020).

The operational sequence of the axial blood pump is depicted in Fig. 1(b), while Fig 1(a) illustrates the important components of the blood pump. Blood enters through the inlet of the pump and passes through the straightener, which is designed to reduce swirl and stabilize the flow before it reaches the impeller, ensuring a uniform flow profile. The impeller, the rotating component of the pump, spins at a constant rpm, imparting kinetic energy to the blood. After passing through the impeller, the blood flows into the diffuser, positioned downstream of the impeller. The diffuser then converts the kinetic energy imparted by the impeller into pressure energy, thereby enhancing the overall efficiency of the pump. Finally, the blood exits through the outlet of the pump.

The geometric specifications of the base model are detailed in Table 1, outlining the foundational design parameters of axial blood pump.

2.2 Computational Domain

The computational domain and interfaces of the pump, as depicted in the accompanying Fig. 2, is designed to capture the flow behavior and accurately simulate the pump's performance. Interfaces_1-2 and 2-1 are defined between the straightener and impeller, while interfaces_2-3 and 3-2 are defined between the impeller and diffuser, as shown in Fig. 2(b). These interfaces are crucial for accurate simulation, as the impeller rotates while the

Table 1 Geometric specifications of the base model (Su et al., 2012; Peng et al., 2014)

S No.	Component	Length (mm)	Number of Blades	Blade Height (mm)
1.	Straightener	20	3	2.5
2.	Impeller	20	2	2.5
3.	Diffuser	20	3	2.5
4.	Assembly	60	8	-

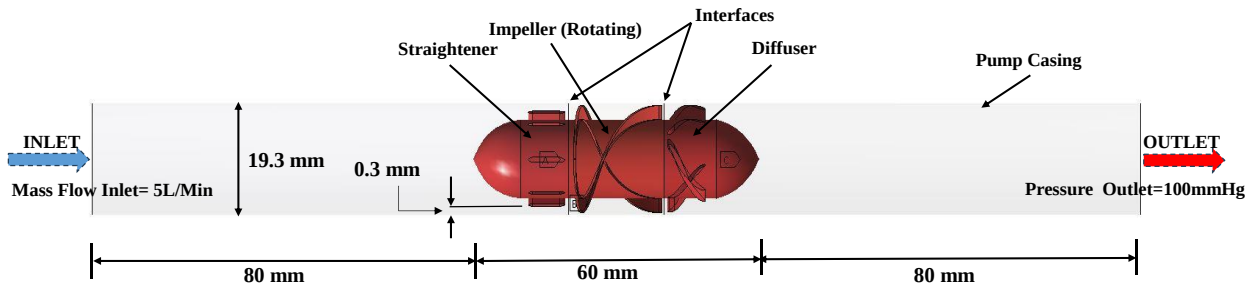

(a) Computational domain for blood pump

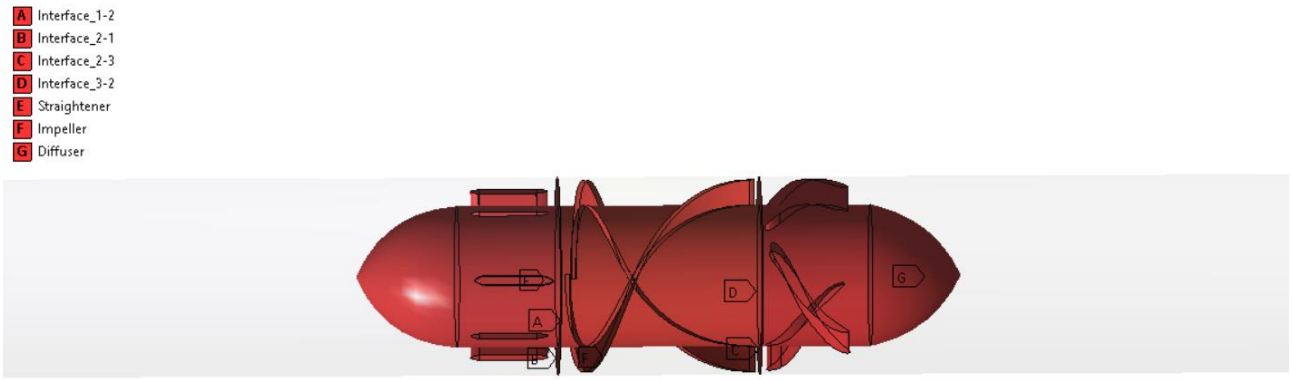

(b) Interfaces of the blood pump

Fig. 2 Computational domain and interfaces of the blood pump

straightener and diffuser remain stationary. The clearance of 0.3 mm is given to blade tip height and the pump casing. To ensure the accuracy of the simulation, the length of the computational domain is extended on both sides by 80 mm. This extension allows for a more comprehensive analysis of the flow characteristics and helps mitigate any potential boundary effects.

2.3 Governing Equations

In CFD simulations, the Navier-Stokes equations are solved using discretized grids in both space and time. When simulating VADs, the fluid flow, which is blood flow in this case, is considered as Newtonian and incompressible (Romanova et al., 2022; Gao et al., 2023). Furthermore, external body forces are typically neglected. With these assumptions in place, the continuity and Navier-Stokes equations can respectively be simplified to the following form:

$$\nabla.\vec{u} = 0 \tag{1}$$

$$\rho\left(\frac{\partial\vec{u}}{\partial t} + \vec{u}.\nabla\vec{u}\right) = -\nabla p + \mu\nabla^2\vec{u} \tag{2}$$

In the presented context, where ρ represents the fluid density, $\vec{u}$ denotes the spatial velocity vector (x, y, z, t) of fluid, t signifies time, p represents pressure, and μ represents dynamic viscosity, Equations (1) and (2) play crucial roles in capturing the conservation of mass and momentum, respectively. These equations form the basis for CFD simulations of VADs, allowing for the analysis of fluid flow characteristics and performance.

2.4 Grid Generation

The initial step in solving flow problems using the finite volume method (FVM) involves generating grids with approximate orthogonality and skewness at the boundaries. For the simulation of the axial blood pump geometry, the ICEM-CFD module available in the Ansys Fluent is utilized to generate the mesh.

The grid generation process involved replicating the geometrical boundaries of the flow domain as specified by the user. Automatic meshing with appropriate element settings is employed in the present study, as depicted in Fig. 3. The number of cells across the gap are set to 10 to ensure sufficient resolution in this region. To maintain grid quality, particular attention is given to the near-wall region. The y+ value of the grids in this region is maintained around 1, aiming to achieve an optimal balance between accuracy and computational efficiency. By employing these grid generation techniques, the computational domain is discretized effectively, enabling accurate analysis of fluid flow within the axial blood pump.

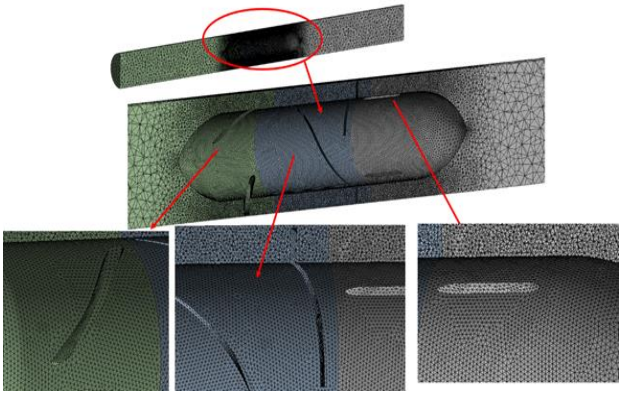

Fig. 3 Grid generation in computational domain

Table 2 Pressure head results for different grid counts

Number of Elements	Pressure Head (mmHg)
912002	112.12
1193085	109.05
1438664	106.01
1635941	107.00

2.5 Grid Independence Test

A grid independence test is performed to assess the sensitivity of the simulation results to the grid resolution. The simulation results are provided in Table 2.

The test focused on evaluating the pressure head across the blood pump, as illustrated in Fig. 4. The objective is to determine the grid size required to achieve accurate results while considering computational resources. The test revealed that the pressure head difference, compared to the finest model, remained below 1% as the numerical model's grid count increased to near 1.48 million. This finding indicated that further grid refinement did not significantly impact the pressure head results. Therefore, the model with 1.48 million grids was deemed a suitable compromise between accuracy and computational resources. By selecting an appropriate grid resolution, the simulation could achieve reliable results while optimizing computational efficiency. The chosen grid size ensured an acceptable level of accuracy in capturing the pressure head across the blood pump, allowing for meaningful analysis of the pump performance and flow dynamics.

2.6 Boundary Condition

Boundary conditions play a pivotal role in accurately simulating the behavior of an axial blood pump. They provide essential details for modeling fluid flow and pressure distribution by specifying conditions at the inlet and outlet boundaries. For the simulation of the axial blood pump, specific boundary conditions are applied. The mass flow rate at the inlet is set to 5 L/min to represent the prescribed flow rate into the pump, ensuring a consistent and controlled blood flow. At the outlet, the pressure is maintained at 100 mmHg, simulating the physiological pressure that the pump needs to overcome for proper blood circulation.

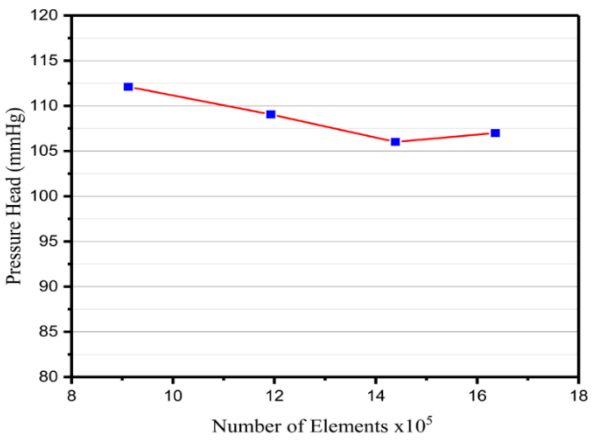

Fig. 4 Grid independence test

Another critical parameter is the impeller rotational speed, which dictates the speed at which the impeller blades revolve within the pump. It significantly influences fluid flow behavior and pressure distribution within the pump system. Varying the impeller rotational speed throughout simulations allows for the investigation of different operational conditions and provides insights into optimal speed ranges for desired pump performance.

Interfaces as shown in Fig. 2(b), also play a vital role in accurately capturing the axial blood pump's behavior during simulation. They define connections between pump components, ensuring seamless flow and pressure transfer. Well-defined interfaces enable appropriate coupling and interaction between the rotating impeller and stationary parts, accurately representing flow dynamics and pressure distribution.

In this study, blood is assumed to exhibit Newtonian behavior, with a viscosity of 0.0035 Pa•s and a density of 1050 kg/m³, as it behaves as a Newtonian fluid at higher shear rates (>100/s) (Nammakie et al., 2017; Wiegmann et al., 2018, 2019), which are typically encountered within the blood pump (Thamsen et al., 2015; Romanova et al., 2022; Gao et al., 2023). This assumption simplifies the simulation process and aligns with blood's behavior under physiological conditions. These boundary conditions, including the constant Newtonian behavior of blood, ensure consistency across simulations and are crucial for accurately capturing flow behavior and pressure distribution within the axial blood pump, providing inputs for realistic and reliable results. Additionally, the SST k-ω model has been selected as the turbulence model, which is well-suited for simulating VADs (Al-Azawy et al., 2016; Wang et al., 2019). A carefully chosen time step size allows for the precise capture of impeller dynamics during unsteady simulations. The time step for computations in the CFD solver, considering the second-order implicit transient formulation, has been selected to capture the minimum movement of the impeller while ensuring accurate results. The aim was to capture the minimum movement of the impeller, ensuring precision in results while also being mindful of computational cost. In addition, smaller impeller movements were computed to assess result variations after seven complete impeller rotation. The time step size was chosen to accurately capture the impeller's minimum movement while balancing accuracy and computational cost. It is calculated using the formula (60 * 5 / impeller rotational speed in rpm * 360). For an impeller rotation speed of 9500 rpm, the time step value is 8.77×10^{-5} sec. This choice ensures precision and has been validated through time-independent and grid independence studies. The final choice of a 5 degree impeller movement in the paper accounts for these considerations. Further, convergence is deemed achieved when the residual values for all equations reach a threshold of 1×10^{-5}.

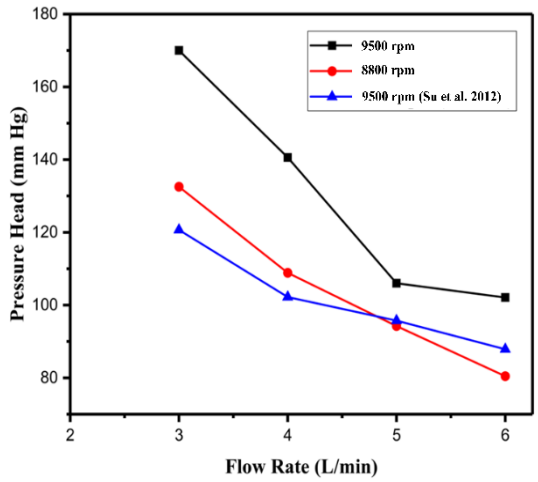

Fig. 5 Validation with literature

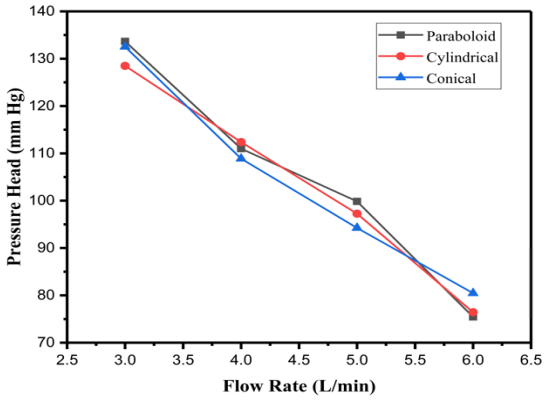

Fig. 6 P-Q curves for different straighteners designs

2.7 Validation with Literature

The validation of the base axial blood pump model is conducted in comparison with relevant literature. The base model, derived from the literature, exhibits interesting findings regarding pressure head generation at different rotating speeds. At 9500 rpm, the base model demonstrates higher pressure head compared to the literature model. However, upon reducing the speed to 8800 rpm, the base model aligns with the literature model, resulting in similar pressure head values. The base model consistently follows the trend observed in the literature, with discrepancies within a 10 percent error margin.

Figure 5, visually represents the comparison between the base model and the literature model. The observed differences may be attributed to certain assumptions made during the modeling process of the base design, which are absent in the literature model. Notably, the reduced rotating speed of 8800 rpm in the base model achieves a flow rate of 5 liters per minute, a performance level similar to that achieved by the literature model at 9500 rpm. This distinction is significant as it indicates a potential reduction in wall shear stress within the pump, thereby enhancing its hemodynamic characteristics.

In conclusion, the validation of the base axial blood pump model, inspired by the literature, demonstrates its capability to replicate the performance trends observed in relevant studies. By achieving a comparable flow rate at a lower rotating speed, the base model exhibits the potential to improve hemodynamic conditions and reduce wall shear stress, contributing to a more favorable hemodynamically sound pump design.

3. RESULTS

This section summarizes the findings from an analysis of three distinct straightener designs for axial blood pumps: paraboloid, conical, and cylindrical. The primary focus areas include pressure head variation, wall shear stress distribution, wall shear stress contours, average wall shear variation on various components, pressure contours, turbulent kinetic energy, and hydraulic performance.

3.1 Pressure Head Variation

The pressure head and flow rate (P-Q Curve) variations for the blood pump with the three different straightener designs are illustrated in Fig. 6. The graph representing the paraboloid design consistently exhibits higher or comparable pressure head compared to the other two designs, particularly at 8800 rpm within the working flow rate range of 3-5 liters per minute, except at 6 liters per minute. In contrast, the pump with the cylindrical and conical straighteners demonstrates slightly lower pressure head values. The results indicate that the paraboloid straightener design performs favorably.

3.2 Wall Shear Stress Distribution in Different Straightener Designs

Wall shear stress variation is a crucial aspect to analyze in order to assess the performance of different straightener designs in axial blood pumps. This section focuses on the wall shear stress distribution for three specific straightener designs: paraboloid, conical, and cylindrical.

3.2.1 Axial blood pump with paraboloid straightener

Figure 7(a) depicts the distribution of count and wall shear stress percentages for the blood pump with a paraboloid straightener. The graph shows that a significant proportion, approximately 98.8%, of the pump regions exhibit wall shear stress values within the threshold of 400 Pa (Sallam & Hwang, 1984). This finding is highly advantageous from a hematological standpoint, as it suggests that the design effectively minimizes the risk of hemodynamic complications. Additionally, Fig. 7(b) shows a scatter plot for the blood pump with the paraboloid straightener, providing further visual representation of the favorable wall shear stress distribution achieved by this design.

The scatter plot reveals that the wall shear stress is maximized near the interfaces of the straightener and impeller, as well as the interface of the impeller and diffuser. This consistent observation is significant and highlights the need for careful design considerations for the impeller blade profile, particularly at its leading and trailing edges, as well as the leading edge of the diffuser. By addressing these areas, it becomes possible to

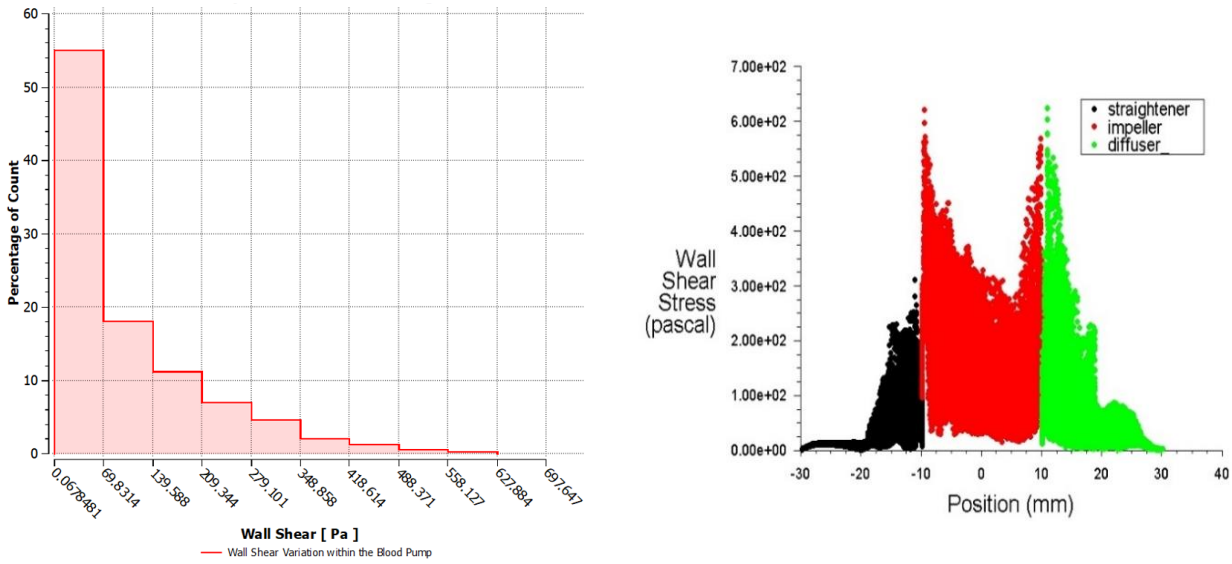

(a) Percentage of Count (b) Scatter Plot

Fig. 7 Wall shear stress variation for blood pump with paraboloid straightener

minimize the sudden spikes of wall shear stress near the interfaces of the pump, ultimately improving the pump's overall performance and reducing the risk of hemodynamic complications.

3.2.2 Axial Blood Pump with Conical Straightener

Figure 8(a) demonstrates the distribution of count and wall shear stress percentages for the blood pump with a conical straightener. The figure reveals that approximately 97.7% of the pump regions exhibit wall shear stress values within the range of 400 Pa, indicating a favorable shear stress level. This finding suggests that the pump with the conical straightener is suitable from a hematological perspective, promoting optimal hemodynamic conditions. It is worth noting, however, that the percentage of count within this range is slightly lower compared to the pump with the paraboloid straightener. Figure 8(b) complements this information by presenting a scatter plot specifically for the blood pump with the conical straightener, providing a visual representation of the shear stress distribution achieved by this design.

The similar trend is observed as are observed in the previous case. The scatter plot highlights that the wall shear stress is also maximized near the interface of the straightener and impeller, as well as at the interface of the impeller and diffuser. This consistent pattern emphasizes the importance of paying close attention to the design of the impeller blade profile, specifically its leading and trailing edges, along with the leading edge of the diffuser. By optimizing these areas, it is possible to minimize the abrupt increases in wall shear stress near the pump's interfaces, leading to improved performance and reduced hemodynamic complications.

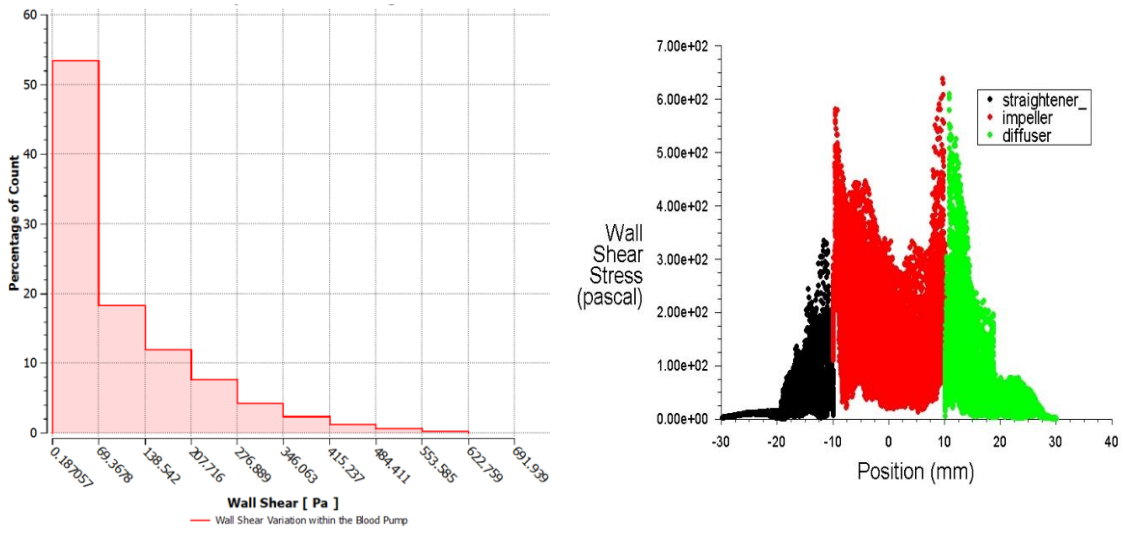

(a) Percentage of Count (b) Scatter Plot

Fig. 8 Wall shear stress variation for blood pump with conical straightener

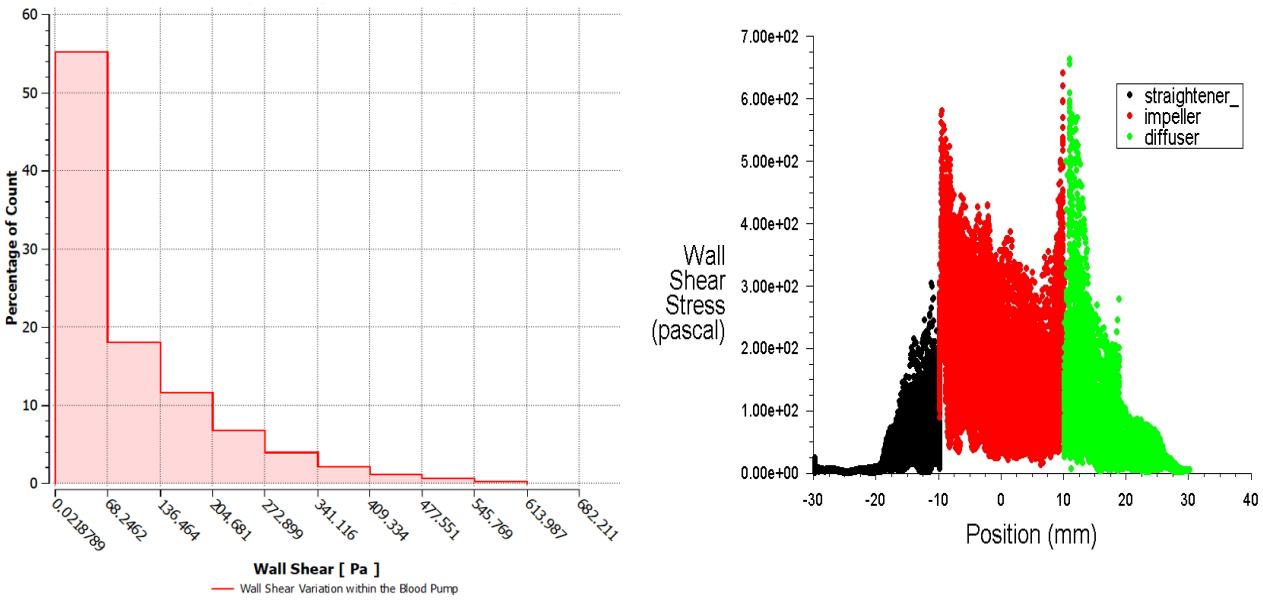

(a) Percentage of Count (b) Scatter Plot

Fig. 9 Wall shear stress variation for blood pump with cylindrical straightener

3.2.3 Axial Blood Pump with Cylindrical Straightener

Figure 9(a) presents the percentage distribution of the count and wall shear stress of the blood pump with the cylindrical straightener. It demonstrates that approximately 98.16% of the pump regions exhibit a wall shear stress within the range of 400 Pa. This result indicates that the pump with the cylindrical straightener is also suitable from a hematological perspective, as it helps to minimize excessive shear stress on the blood. However, it should be noted that the percentage of count is slightly lower than that of the pump with the paraboloid straightener. Additionally, Fig. 9(b) displays the scatter plot for the blood pump with the cylindrical straightener.

Similar to the previous cases, the scatter plot demonstrates that the wall shear stress is highest near the interface of the straightener and impeller, as well as at the interface of the impeller and diffuser. This consistent observation highlights the critical role of the impeller blade profile, particularly its leading and trailing edges, along with the leading edge of the diffuser, in minimizing sudden spikes of wall shear stress near the pump's interfaces. By focusing on these design aspects, it is possible to optimize the pump's performance, reducing the risk of hemodynamic complications.

In summary, the scatter plots reveal a consistent trend for each case. The maximum wall shear stress occurs near the interfaces of the straightener and impeller, as well as the interface of the impeller and diffuser. This emphasizes the significance of carefully designing the impeller blade profile and the leading edge of the diffuser to minimize these sudden spikes of wall shear stress near the pump's interfaces. By addressing these design considerations, the overall performance of the blood pump can be improved, and the risk of hemodynamic complications can be mitigated.

3.3 Wall Shear Stress Contour

Figure 10 shows the wall shear stress contours calculated after 7 complete rotations of the impeller, with a flow rate of 5 L/min and a pressure of 100 mmHg, reflecting normal human physiological conditions at an impeller speed of 8800 rpm. This contour map illustrates the distribution of wall shear stress across the entire blood pump component, allowing for a comparison between different straightener designs.

In the case of the pump with the cylindrical straightener, the contours illustrate that the shear stress is concentrated more prominently on the diffuser blades' leading edge and near the impeller and diffuser interface. This indicates a higher level of shear stress in these regions compared to the other designs.

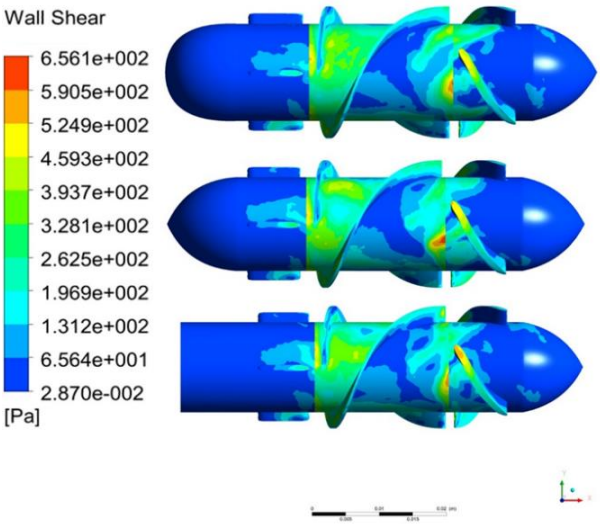

Fig. 10 Wall shear stress distribution with different straighteners

Similarly, the conical straightener design exhibits a similar distribution of shear stress, with slightly lower shear stress observed at the leading edge of the diffuser blades. However, the overall pattern remains consistent with higher shear stress near the impeller and diffuser interface.

On the other hand, the pump with the paraboloid straightener demonstrates the lowest concentration of wall shear stress on the diffuser blades. The contours indicate a significant reduction in shear stress on the diffuser blades compared to the other designs. This suggests that the paraboloid shape plays a role in minimizing the overall concentration of wall shear stress on the diffuser blades.

Overall, the wall shear stress contours highlight that the cylindrical and conical straighteners exhibit a relatively higher concentration of shear stress in specific regions, particularly near the impeller and diffuser interface. In contrast, the paraboloid straightener design demonstrates a more favorable distribution with the lowest concentration of shear stress on the diffuser blades.

3.4 The Average Wall Shear Stress Variation on the Components of the Blood Pump

The average wall shear stress variation across different components of the blood pump is analyzed to provide insights into the hemodynamic performance and potential complications. The average wall shear stress is computed using the integral formula:

$$\tau_{avg} = \frac{1}{A}\int_A \tau_\omega dA \tag{3}$$

Where τ_{avg} is the average wall shear stress, A is the total surface area of the component, τ_ω is the wall shear stress at a differential area *dA*.

The average wall shear variation on the components of the blood pump may provide valuable insights into the hemodynamic characteristics of the pump. By analyzing the distribution of average wall shear stress on individual components and different regions, it can assessed the potential for blood cell damage, clot formation, and other related complications.

It is important to note that the precise wall shear stress values will depend on the pump's design features and operating circumstances. Different parts of the blood pump, such as the straightener, impeller, and diffuser, might have differing average wall shear stresses. Individuals may identify regions with greater or lower shear stress and evaluate the effects by analysing the wall shear stress on these components. The variation of average wall shear stress in individual components are discussed in subsequent sub-section.

3.4.1 Average Wall Shear Stress Variation on Straightener

The average variation of wall shear stress on different straighteners of the blood pump is depicted in Fig. 11. The figure demonstrates the average wall shear stress variation with respect to the flow rate. For all the blood pumps with different straighteners, the average wall shear stress values remain below 70 Pa. Among the three designs, the pump with the cylindrical straightener exhibits the lowest average wall shear stress for all of the flow rate ranges.

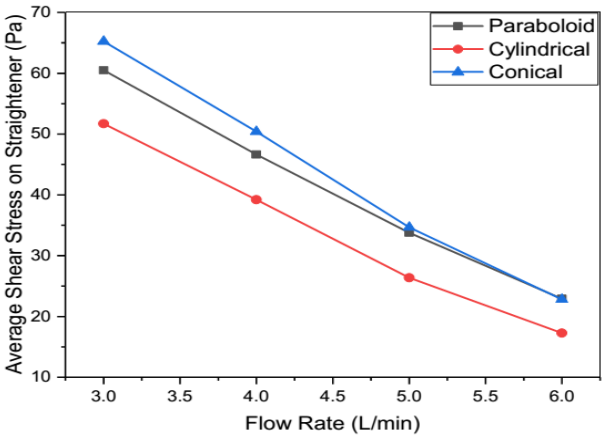

Fig. 11 Average wall shear stress variation on straightener for different flow rates

Conversely, the pump with the conical straightener shows the highest average wall shear stress values across all of the flow rate ranges. The pump with the paraboloid straightener falls in between the cylindrical and conical designs, with intermediate average wall shear stress values. Additionally, the graph illustrates that as the flow rate increases, the average wall shear stress continuously decreases. This trend suggests that the higher flow rates result in reduced wall shear stress on each of the straightener designs of the blood pump.

It can be concluded based on Fig. 11, that the values of the average wall shear stress observed below a threshold value of 70 Pa for all of the pump designs indicating favorable conditions in terms of average wall shear stress for the straighteners. However, it is important to note that other components, such as the impeller and diffuser, play crucial roles and require further analysis. The next section will delve into the detailed examination of these components and their impact on the overall performance of the pump.

3.4.2 Average Wall Shear Stress Variation on Impeller

The average wall shear stress variation for the impeller of the pump is presented in Fig. 12. The graph illustrates that the values for all designs remain below 200 Pa across the flow rate ranges. Specifically, the pump with the cylindrical straightener exhibits the lowest average wall shear stress values among all of the designs for all flow rate ranges. On the other hand, the pumps with the conical and paraboloid straighteners display similar trends, with average wall shear stress values in close proximity across the flow rate ranges. Considering that all designs maintain average wall shear stress values below 200 Pa, it can be inferred that all designs are suitable in terms of clinical performance

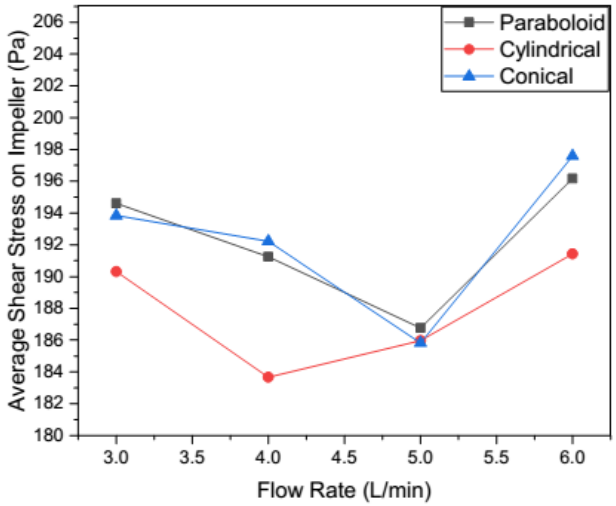

Fig. 12 Average wall shear stress variation with flow rate for different impellers

based on this graph. However, it is important to consider other factors such as turbulent kinetic energy and the presence of high-concentration zones of wall shear stress when assessing the overall clinical performance of the pump.

3.4.3 Average Wall Shear Stress Variation on Diffuser

The variation of average wall shear stress with flow rate for different diffuser geometries is depicted in Fig. 13. The figure reveals an interesting trend that differs from the variation observed in the case of straightener region. This shows that as the flow rate increases, the average wall shear stress in the diffuser region also increases.

Specifically, the pump with the cylindrical straightener and the conical straightener exhibit a more pronounced increase in average wall shear stress in the diffuser region as the flow rate increases. In contrast, the pump with the paraboloid straightener demonstrates a relatively smaller increase in average wall shear stress in the diffuser region compared to the other two designs. This suggests that the pump with the paraboloid straightener performs better in terms of minimizing the increase in average wall shear stress with increasing flow rate.

These findings highlight the importance of paying attention to the design of the diffuser when developing the pump. Since the average wall shear stress in the diffuser region shows a correlation with flow rate, careful consideration of the diffuser design can help optimize the pump's performance and minimize potential hemodynamic complications.

3.5 Pressure Contour

The pressure contours due to change in geometry of the blood pump with paraboloid, conical, and cylindrical straighteners are displayed in Fig. 14. The blood pump with the cylindrical straightener exhibits a more concentrated pressure on the trailing edge of the impeller blade profile compared to the other

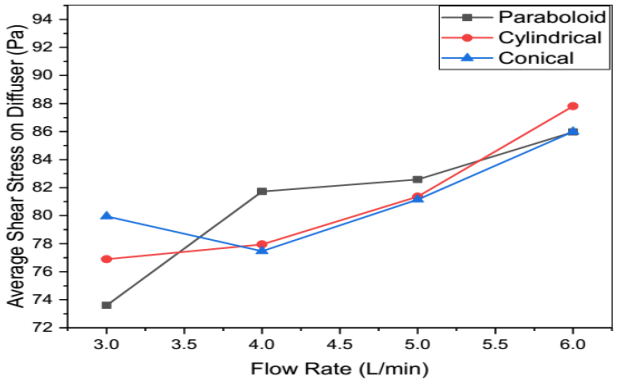

Fig. 13 Average wall shear stress variation on diffuser

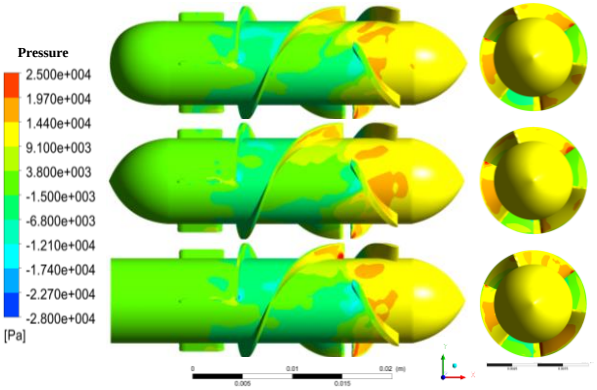

Fig. 14 Pressure contour for blood pump with different straightener geometries

two designs. In contrast, the pumps with the paraboloid and conical straighteners demonstrate lower pressure on the blade surfaces compared to the cylindrical straightener.

When examining the radial view, it is evident that both the paraboloid and cylindrical straighteners generate lower pressure than the pump with the cylindrical straightener. This indicates that the paraboloid straightener design may be more suitable from a clinical perspective.

Overall, the pressure contours highlight the differences in pressure distribution among the three straightener designs. The paraboloid straightener design, in particular, shows a more favorable pressure profile, suggesting its potential benefits in terms of clinical aspects.

3.6 Turbulent Kinetic Energy

The contours of turbulent kinetic energy for the three pumps with different straightener designs are depicted in the Fig. 15. In the case of the pump with the cylindrical straightener, a significant concentration of turbulent kinetic energy is observed on the leading edge of the diffuser blades, as indicated by the contour plot. Similarly, the pump with the conical straightener exhibits a high concentration of turbulent kinetic energy on both the leading edge of the diffuser blades and the hub near the impeller-diffuser interface, as shown in the contour plot.

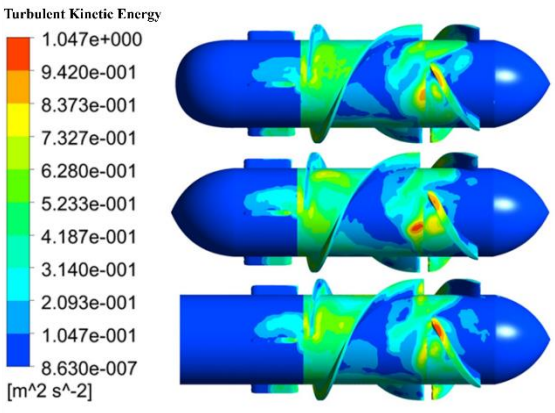

Fig. 15 Turbulent kinetic energy contour for blood pump with different straightener geometries

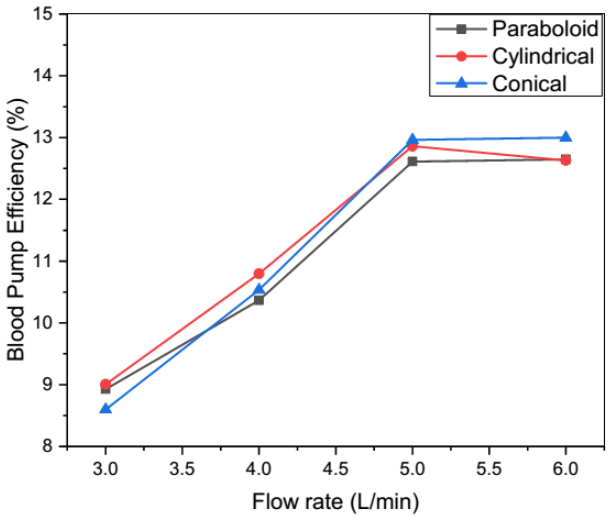

Fig. 16 Blood pump efficiency

In contrast, the pump with the paraboloid straightener displays a relatively lower intensity of turbulent kinetic energy on the leading edge of the diffuser blades and the hub near the impeller-diffuser interface, as depicted in the figure. The pattern observed for the paraboloid shape is similar to the conical shape, but the intensity of turbulent kinetic energy is the lowest in the case of the paraboloid straightener. On the other hand, the cylindrical shape exhibits the highest intensity of turbulent kinetic energy on the diffuser blades.

Considering these findings, the paraboloid straightener design is more preferable choice for the blood pump applications. It demonstrates a lower intensity of turbulent kinetic energy, suggesting a substantial reduction in the potential hemodynamic complications associated with high turbulence levels.

3.7 Hydraulic Performance

The hydraulic performance of the blood pump with three different straighteners, namely conical, paraboloid, and cylindrical, was numerically computed at a rotating speed of 8800 rpm and a flow rate of 5 liters per minute. The plot in Fig. 16 displays the relationship between efficiency and flow rate, ranging from 3 to 6 liters per minute. The efficiency values varied from approximately 8.5% to 13% within this flow rate range. For the specific flow rate of 5 liters per minute, the hydraulic efficiencies achieved were 12.9%, 12.6%, and 12.8% for the conical, paraboloid, and cylindrical straighteners, respectively. These efficiency values observed were consistent with those reported in the literature. For instance, Peng et al. (2014) reported an efficiency of 14% with a six-blade impeller configuration, while our simulations achieved comparable results with a three-blade impeller. Similarly, our findings align closely with Song et al. (2004), who reported 13% efficiency for the UAP-1 axial blood pump. These comparisons demonstrate the robustness and accuracy of our simulation results across different design contexts.

It is worth noting that the pump with the paraboloid straightener exhibited the lowest hydraulic efficiency among the three designs. However, it is important to highlight that the pump with the paraboloid straightener was capable of generating higher pressure at this specific operating condition, which is a positive outcome. While the hydraulic efficiency may be slightly lower, the ability to develop increased pressure can be advantageous in certain clinical scenarios.

4. CONCLUSION

In this article, a comprehensive analysis of the impact of different straightener designs on the overall performance of axial blood pumps is conducted. The goal was to evaluate the performance of three different straightener profiles: conical, cylindrical, and paraboloid shapes. Various performance parameters, including pressure rise, wall shear stress, turbulent kinetic energy, and hydraulic efficiency were compared.

The study revealed several important findings. Firstly, the pump with the paraboloid straightener consistently exhibited higher or comparable pressure head values compared to the other two designs. This indicates that the paraboloid straightener design performs favorably in terms of generating the required pressure for effective blood circulation.

Secondly, all designs maintained wall shear stress values below 400 Pa in most regions within the pump. The pump equipped with the paraboloid straightener demonstrated the lowest concentration of wall shear stress, with 98.8% within the pump, while pumps with conical and cylindrical shapes showed 97.7% and 98.16% respectively. Additionally, the pump with the paraboloid straightener exhibited the lowest concentration of wall shear stress on the diffuser blades. This suggests its potential to minimize hemodynamic complications associated with excessive wall shear stress.

Furthermore, the analysis of turbulent kinetic energy indicated that the pump with the paraboloid straightener demonstrated a lower intensity of turbulence compared to the other designs. This suggests

a potential reduction in hemodynamic complications, primarily associated with thrombogenic events linked to high turbulence levels.

Considering the findings from the pressure head, wall shear stress, turbulent kinetic energy analyses, and hydraulic efficiency, the paraboloid straightener design emerges as a suitable choice for the blood pump application. While it may have a slightly lower hydraulic efficiency compared to the other designs, its ability to generate higher pressure, with lesser wall shear stress, and reduced turbulence levels highlights its potential to enhance the clinical performance of the pump. These findings contribute to the ongoing efforts in optimizing pump design and improving the performance of axial blood pumps, ultimately benefiting patients with cardiovascular diseases. Future research may focus on refining the straightener design and investigating the impact of other pump components on overall performance.

5. FUTURE SCOPE

The current study provides valuable insights into the performance of axial flow blood pumps with different straightener designs. However, several avenues for future research could further enhance the understanding and optimization of these devices. Future work could explore innovative straightener geometries to potentially improve flow stabilization, pressure head, and durability, while also reducing hemodynamic complications. Although current simulations have used a constant impeller rotational speed, future research could make significant step by examining variable impeller speeds (speed modulation) to generate pulsatile outflow. This would offer deeper insights into pump performance across different operational phases and more accurately replicate physiological conditions. Additionally, employing advanced optimization techniques, such as genetic algorithms or machine learning, could uncover optimal configurations for straighteners, impellers, and diffusers, leading to enhanced performance and minimized adverse effects.

Further research should include developing patient-specific computational models to tailor pump designs to individual anatomical variations, conducting detailed hemocompatibility studies, and assessing long-term performance and reliability. Integrating multiphysics simulations to examine the interaction between fluid dynamics and mechanical components can guide better design and material choices. Additionally, addressing regulatory and clinical pathways, along with experimental validation of simulation results, is crucial for real-world applicability and compliance with medical standards. Exploring new straightener geometries and microscale cell-solid interactions, as discussed in literature (Silva et al., 2024), can further advance blood pump design and functionality. By addressing these areas, future research can significantly enhance the development of more efficient, durable, and patient-friendly axial blood pumps, ultimately benefiting patients with heart failure.

CONFLICT OF INTEREST

The authors declare that there is no conflict of interest.

AUTHOR CONTRIBUTIONS

Pravin Kumar Shukla: Conceptualization, Methodology, Software, Data Curation, Visualization, Writing – Original Draft. **Rakesh Mishra:** Supervision, Critical Feedback, Interpretation of Results, Writing – Review & Editing. **R. P. Tewari:** Supervision, Interpretation of Results, Writing – Review & Editing, Project Administration.

REFERENCES

Al-Azawy, M. G., Turan, A., & Revell, A. (2016). Assessment of turbulence models for pulsatile flow inside a heart pump. *Computer Methods in Biomechanics and Biomedical Engineering*, *19*(3), 271–285. https://doi.org/10.1080/10255842.2015.1015527

Bounouib, M., Benakrach, H., Es-Sadek Zeriab, M., Taha-Janan, M., & Maazouzi, W. (2020). Numerical study of a new ventricular assist device. *Artificial Organs*, *44*(6), 604–610. https://doi.org/10.1111/aor.13635

Cheng, L., Tan, J., Yun, Z., Wang, S., & Yu, Z. (2021). Analysis of flow field and hemolysis index in axial flow blood pump by computational fluid dynamics–discrete element method. *The International Journal of Artificial Organs*, *44*(1), 46–54. https://doi.org/10.1177/0391398820917145

Gao, X., Xu, Z., Chen, C., Hao, P., He, F., & Zhang, X. (2023). Full-scale numerical simulation of hemodynamics based on left ventricular assist device. *Frontiers in Physiology*, *14*, 1192610. https://doi.org/10.3389/fphys.2023.1192610

Jou, S., Mendez, S. R., Feinman, J., Mitrani, L. R., Fuster, V., Mangiola, M., Moazami, N., & Gidea, C. (2024). Heart transplantation: Advances in expanding the donor pool and xenotransplantation. *Nature Reviews Cardiology*, *21*(1), 25–36. https://doi.org/10.1038/s41569-023-00902-1

Kannojiya, V., Das, A. K., & Das, P. K. (2019). Proposal of hemodynamically improved design of an axial flow blood pump for LVAD. *Medical & Biological Engineering & Computing*, 1–18. https://doi.org/10.1007/s11517-019-02097-5

Mani, T., Yeldose, M., Mannamplackal, T. J., Joy, J., & Jacob, R. G. (2021). Axial ventricular assist devices: A review focused on magnetic levitation, speed control and packaging. *Materials Today: Proceedings*, *47*, 5379–5385. https://doi.org/10.1016/j.matpr.2021.06.090

Nammakie, E., Niroomand-Oscuii, H., Koochaki, M., & Ghalichi, F. (2017). Computational fluid dynamics-based study of possibility of generating pulsatile

blood flow via a continuous-flow VAD. *Medical & Biological Engineering & Computing*, *55*(1), 167–178. https://doi.org/10.1007/s11517-016-1523-8

Noly, P. E., Pagani, F. D., Noiseux, N., Stulak, J. M., Khalpey, Z., Carrier, M., & Maltais, S. (2020). Continuous-flow left ventricular assist devices and valvular heart disease: A comprehensive review. *Canadian Journal of Cardiology*, *36*(2), 244–260. https://doi.org/10.1016/j.cjca.2019.11.022

Peng, Y., Wu, Y., Tang, X., Liu, W., Chen, D., Gao, T., Xu, Y., & Zeng, Y. (2014). Numerical simulation and comparative analysis of flow field in axial blood pumps. *Computer Methods in Biomechanics and Biomedical Engineering*, *17*(7), 723–727. https://doi.org/10.1080/10255842.2012.715156

Qi, J., Zhou, Y., Wang, D., & Zhong, L. (2012). Numerical analysis of an axial blood pump with different impeller blade heights. *Journal of Mechanics in Medicine and Biology*, *12*(03), 1250045. https://doi.org/10.1142/S0219519411004629

Romanova, A. N., Pugovkin, A. A., Denisov, M. V., Ephimov, I. A., Gusev, D. V., Walter, M., Groth, T., Bockeria, O. L., Le, T. G., & Satyukova, A. S. (2022). Hemolytic performance in two generations of the sputnik left ventricular assist device: A combined numerical and experimental study. *Journal of Functional Biomaterials*, *13*(1), 7. https://doi.org/10.3390/jfb13010007

Sallam, A. M., & Hwang, N. H. (1984). Human red blood cell hemolysis in a turbulent shear flow: Contribution of Reynolds shear stresses. *Biorheology*, *21*(6), 783–797. https://doi.org/10.3233/BIR-1984-21605

Shukla, P. K., Mishra, R., & Tewari, R. P. (2023). Analysis of rotary ventricular assist devices using CFD technique—A review. *Proceedings of the Institution of Mechanical Engineers, Part E: Journal of Process Mechanical Engineering*, *237*(3), 1036–1063. https://doi.org/10.1177/09544089221128366

Silva, D. P. F., Coelho, R. C. V., Pagonabarraga, I., Succi, S., Gama, M. M. T. da, & Araújo, N. A. M. (2024). Lattice boltzmann simulation of deformable fluid-filled bodies: progress and perspectives. *Soft Matter*, *20*(11), 2419–2441. https://doi.org/10.1039/D3SM01648J

Song, X., Untaroiu, A., Wood, H. G., Allaire, P. E., Throckmorton, A. L., Day, S. W., & Olsen, D. B. (2004). Design and transient computational fluid dynamics study of a continuous axial flow ventricular assist device. *ASAIO Journal*, *50*(3), 215–224. https://doi.org/10.1097/01.mat.0000124954.69612.83

Su, B., Chua, L. P., & Wang, X. (2012). Validation of an axial flow blood pump: Computational fluid dynamics results using particle image velocimetry: Validation of blood pump using particle image velocimetry. *Artificial Organs*, *36*(4), 359–367. https://doi.org/10.1111/j.1525-1594.2011.01362.x

Thamsen, B., Blümel, B., Schaller, J., Paschereit, C. O., Affeld, K., Goubergrits, L., & Kertzscher, U. (2015). Numerical analysis of blood damage potential of the heartmate II and heartware HVAD rotary blood pumps: Blood damage potential of blood pumps. *Artificial Organs*, *39*(8), 651–659. https://doi.org/10.1111/aor.12542

Tu, J., Xu, L., Li, F., & Dong, N. (2024). Developments and challenges in durable ventricular assist device technology: A comprehensive review with a focus on advancements in china. *Journal of Cardiovascular Development and Disease*, *11*(1), 29. https://doi.org/10.3390/jcdd11010029

Untaroiu, A., Throckmorton, A. L., Patel, S. M., Wood, H. G., Allaire, P. E., & Olsen, D. B. (2005). Numerical and experimental analysis of an axial flow left ventricular assist device: the influence of the diffuser on overall pump performance. *Artificial Organs*, *29*(7), 581–591. https://doi.org/10.1111/j.1525-1594.2005.29095.x

Valledor, A. F., Rubinstein, G., Moeller, C. M., Lorenzatti, D., Rahman, S., Lee, C., Oren, D., Farrero, M., Sayer, G. T., & Uriel, N. (2024). Durable left ventricular assist devices as a bridge to transplantation in the old and the new world. *The Journal of Heart and Lung Transplantation*. https://www.sciencedirect.com/science/article/pii/S105324982400038X

Wang, S., Tan, J., & Yu, Z. (2019). Comparison and experimental validation of turbulence models for an axial flow blood pump. *Journal of Mechanics in Medicine and Biology*, *19*(08), 1940063. https://doi.org/10.1142/S0219519419400633

Wiegmann, L., Boës, S., de Zélicourt, D., Thamsen, B., Schmid Daners, M., Meboldt, M., & Kurtcuoglu, V. (2018). Blood pump design variations and their influence on hydraulic performance and indicators of hemocompatibility. *Annals of Biomedical Engineering*, *46*, 417–428. https://doi.org/10.1007/s10439-017-1951-0

Wiegmann, L., Thamsen, B., De Zélicourt, D., Granegger, M., Boës, S., Schmid Daners, M., Meboldt, M., & Kurtcuoglu, V. (2019). Fluid dynamics in the heartmate 3: influence of the artificial pulse feature and residual cardiac pulsation. *Artificial Organs*, *43*(4), 363–376. https://doi.org/10.1111/aor.13346

Wu, T., Khir, A. W., Kütting, M., Du, X., Lin, H., Zhu, Y., & Hsu, P. L. (2020). A review of implantable pulsatile blood pumps: Engineering perspectives. *The International Journal of Artificial Organs*, *43*(9), 559–569. https://doi.org/10.1177/0391398820902470

Xiang, W. J., Huo, J. D., Wu, W. T., & Wu, P. (2023). Influence of inlet boundary conditions on the

prediction of flow field and hemolysis in blood pumps using large-eddy simulation. *Bioengineering*, *10*(2), 2. https://doi.org/10.3390/bioengineering10020274

Yang, W., Peng, S., Xiao, W., Hu, Y., Wu, H., & Li, M. (2022). CFD-based flow channel optimization and performance prediction for a conical axial maglev blood pump. *Sensors*, *22*(4), 1642. https://doi.org/10.3390/s22041642